Journal of ELECTRONIC MATERIALS, Vol. 45, No. 10, 2016
DOI: 10.1007/s11664-016-4660-9

The Effects of Cd^{2+} Concentration on the Structure, Optical and Luminescence Properties of $MgAl_2O_4$:*x*% Cd^{2+} ($0 < x \leq 1.75$) Nanophosphor Prepared by Sol–Gel Method

S.V. MOTLOUNG,[1,5,6] F.B. DEJENE,[2] M.E. SITHOLE,[1] L.F. KOAO,[2] O.M. NTWAEABORWA,[3] H.C. SWART,[3] and T.E. MOTAUNG[4]

1.—Department of Physics, Sefako Makgatho Health Science University, P. O. Box 94, Medunsa 0204, South Africa. 2.—Department of Physics, University of the Free State (Qwaqwa Campus), Private Bag X13, Phuthaditjhaba 9866, South Africa. 3.—Department of Physics, University of the Free State, P.O. Box 339, Bloemfontein 9300, South Africa. 4.—Department of Chemistry, University of Zululand, Guldengracht st & East Arterial Road, Richards Bay 3900, South Africa. 5.—e-mail: cchataa@gmail.com. 6.—e-mail: setumo.motloung@smu.ac.za

Cadmium-doped magnesium aluminate ($MgAl_2O_4$:*x*% Cd^{2+}) powders with different cadmium concentrations ($0 < x \leq 1.75$) were prepared by the sol–gel method. Energy dispersive x-ray spectroscopy (EDS) analysis confirmed the presence of the expected elements (Mg, Al, O, and Cd). The x-ray diffraction (XRD) analysis revealed that the powders crystallized into the cubic spinel structure. Cd^{2+} doping influenced crystallinity of the powder samples. The crystallite size and particle morphology were not affected by variation in the Cd^{2+} concentration. Ultraviolet–visible spectroscopy (UV–vis) measurements revealed that the band gap of the $MgAl_2O_4$ was influenced by Cd^{2+} doping. Un-doped and Cd^{2+}-doped $MgAl_2O_4$ nanophosphors exhibited violet emission at 392 nm. There was no evidence of the emission peak shift, which suggested that all emissions originated from the defects within the host material. Increasing the Cd^{2+} concentration up-to 0.88 mol.% lead to luminescence intensity enhancement, while further increase of Cd^{2+} concentration lead to concentration quenching. The critical energy transfer distance (R_c) between the neighbouring donors and acceptors was found to be 5.21 Å, suggesting that the multipole–multipole interaction (M-MI) is the major cause of concentration quenching. Commission Internationale de l'Elcairage (CIE) colour coordinates confirmed non-tuneable violet emission with intensity dependent on the Cd^{2+} concentration.

Key words: Sol–gel, $MgAl_2O_4$, Cd^{2+}-doped, luminescence, CIE

INTRODUCTION

Crystalline compounds such as the spinel oxides present a large range of interesting electrical, magnetic, and optical properties.[1] Magnesium-aluminate ($MgAl_2O_4$) spinel has drawn remarkable interest among researchers around the world due to the following properties: high melting point (2135°C), high hardness (7.5–8 Mohs), and interesting thermal and optical properties.[1,2] The $MgAl_2O_4$ spinel structure can be described as a cubic closest-packed array of O atoms, with one eighth of the tetrahedral sites and one half of the octahedral sites filled.[3] Assuming a stoichiometric spinel, the formula may be written as:

$$(Mg_{1-y}Al_y)(Al_{2-y}Mg_y)O_4 \ldots . \quad (1)$$

$MgAl_2O_4$ can crystallize in the "normal" or "inverse" spinel structures. From Eq. 1, the terms "normal" and "inverse" are used to denote spinels

(Received December 17, 2015; accepted May 12, 2016; published online June 2, 2016)

for which $y = 0$ and $y = 1$, respectively. For a completely random distribution of Mg^{2+} and Al^{3+} cations among the tetrahedral and octahedral sites, $y = 0.6667$.[3] In the normal $MgAl_2O_4$ structure, eight magnesium ions (Mg^{2+}) occupy tetrahedral sites and 16 aluminium ions (Al^{3+}) occupy octahedral sites while in the inverse spinel structure, eight Mg^{2+} and eight Al^{3+} interchange position, and the other eight Al^{3+} stay at octahedral sites. The structure disorder is responsible for Al^{3+} in tetrahedral sites and Mg^{2+} in octahedral sites.[4] The space group of $MgAl_2O_4$ is $Fd\bar{3}m(O_h^7)$ and the lattice parameter a equals 8.08435 Å.[3] $MgAl_2O_4$ phosphor has shown efficient luminescence in the presence of intentionally incorporated foreign ions, particularly rare earths (RE's) and transition metal (TM) ions in the crystal lattice.[5] For instance, several investigations based on the RE's[6,7] and TM[8,9] ions doped into $MgAl_2O_4$ (host) have been previously reported in the literature. Jia et al.[6] prepared the $MgAl_2O_4$:Ce^{3+} ceramic samples, which have green persistent phosphorescence of a lifetime longer than 10 h by the sintering method. The long persistent luminescence was attributed to a hole trapped at a divalent site called the V_K^{3+} center in $MgAl_2O_4$. Chen et al.[7] prepared the spherical and rod-like porous $MgAl_2O_4$:Eu^{3+} phosphors via a simple hydrothermal synthesis followed by post-annealing in air at 1100°C for 3 h. The excellent red-emitting property of $MgAl_2O_4$:Eu^{3+} phosphors was attributed to the characteristic transitions of Eu^{3+} ion from $^5D_0 \rightarrow {}^7F_j$ ($j = 0$, 1, 2, 3, and 4). Jouini et al.[8] prepared the square-shaped blue single crystals of $MgAl_2O_4$:Ni^{2+} spinel by the micro-pulling-down method. Under excitation in the red region at 646 nm, the infrared emission spectra exhibit a non-structural broad band peak at around 1240 nm, which was attributed to the $^3T_2$ (^3F) $\rightarrow$ $^3A_2$ (^3F) transition of the octahedrally coordinated Ni^{2+} ion. Singh et al.[9] prepared $MgAl_2O_4$:Mn^{2+} phosphors at 500°C by the combustion route. Photoluminescence studies showed the existence of both green and red emissions, which were originating from two independent luminescence channels. The green emission at 518 nm was attributed to the $^4T_1 \rightarrow {}^6A_1$ transition of Mn^{2+} ions, while the red emission at 650 nm was attributed to the charge-transfer de-excitation associated with the Mn^{2+} ion. One of the non-popular and interesting foreign ions doped into the host lattice of the phosphor that has been investigated or studied is the Cd^{2+} ion. Chen et al.[10] reported the composition and constituent effects (i.e., substitution of Zn^{2+} with different amounts of Cd^{2+} or Ga^{3+} with Al^{3+}) in $ZnGa_2O_4$:Cd^{2+} phosphors. Their results showed that with an increase of Cd^{2+} substitution, the emission and excitation wavelengths of the self-activated $(Zn_{1-x}Cd_x)Ga_2O_4$ exhibits a red shift. These observations were attributed to the systematic narrowing of the energy gap (E_g) of the host, which was attributed to the expansion of the lattice dimensions induced by Cd^{2+} substitution. Moreover, Vijayalakshmi et al.[11] successfully prepared the thin films of ZnO:Cd with different Cd concentrations by the spray pyrolysis method on different substrates at 400°C. They found that the increase in Cd concentration leads to the broadening of the emission peak, while the crystalline quality was observed to degrade. The produced thin films were highly transparent in the visible region, and the absorption edge showed a red shift.

In addition to these studies there is Cd^{2+} doping into the crystal lattice of different host materials (e.g., $ZnGa_2O_4$,[10] and ZnO,[11]). This study is on luminescent properties of Cd^{2+} doped $MgAl_2O_4$, which is essentially motivated by the quest to acquire a deeper insight into the materials nature of $MgAl_2O_4$:x% Cd^{2+} with the possibility of producing more promising oxides of phosphors for the purpose of practical application, such as blue light-emitting diodes (BLEDs). Herein, we report the effects of varying the Cd^{2+} concentration on the structural, morphological, optical and luminescence properties of the un-doped and Cd^{2+}-doped $MgAl_2O_4$ nanophosphors.

EXPERIMENTAL

The un-doped and $MgAl_2O_4$:x% Cd^{2+}($0 < x \leq 1.75$%)nanophosphor were synthesized using a well-known sol–gel technique.[12] A similar experimental flow chart as in Fig. 1 was followed to synthesize nano-powder samples.[12] The host material was prepared by dissolving $Mg(NO_3)_2{\cdot}6H_2O$ (98%), $Al(NO_3)_3{\cdot}9H_2O$ (98.5%), and citric acid (CA) $C_8H_8O_7{\cdot}H_2O$ (99%) in deionized water. The sols stoichiometric molar ratio of Mg:Al was 1:2. Cd^{2+}-doped samples were prepared by adding different concentrations of $Cd(NO_3)_2{\cdot}4H_2O$ (99%) in the range of ($0 < x \leq 1.75$%) into the separate beakers of the host solution. The foreign ion Cd^{2+} was chosen with an objective of enhancing the violet colour of $MgAl_2O_4$ phosphor with an intention of using them for the purposes such as BLEDs. Mg:CA molar ratio was kept constant at 1:0.75 for all samples. The temperature was kept at ~80°C, while constantly stirring using a magnetic stirrer until the solution forms a gel. The gels were dried in an oven at 130°C, and ground to get powders. The powder samples were subsequently fired at 800°C in a furnace for 1 h. The powder products were crushed once again for the analysis with different techniques.

The crystal structure and phase composition of the samples were characterized by a powder x-ray diffraction (XRD) (Bruker AXS Discover diffractometer) with CuKα (1.5418 Å) radiation. The elementary composition and surface morphology of the phosphor powder were investigated using a Shimadzu Superscan ZU SSX-550 electron microscope (SEM) with energy dispersion spectroscopy (EDS). High-resolution transmission electron microscopy (HR-TEM) was performed with a JEOL JEM 2100

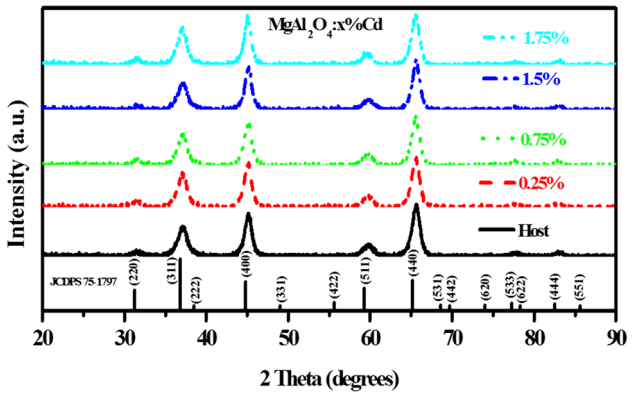

Fig. 1. The XRD pattern for the un-doped and *x*% Cd^{2+}-doped $MgAl_2O_4$ samples at the varying Cd^{2+} concentration.

containing a LaB_6 filament. Diffuse reflectance spectra were recorded using a Lambda 950 UV–vis spectrophotometer with an integrating sphere using spectralon as a reflectance standard. Room temperature photoluminescence (PL) measurements were done using a Hitachi F-7000 fluorescence spectrophotometer.

RESULTS AND DISCUSSION

The phase purity and crystal structure of the sol–gel synthesized powder samples were analysed by the XRD method. The XRD patterns of the un-doped and Cd^{2+}-doped $MgAl_2O_4$ are shown in Fig. 1. The XRD measurements revealed that the powder samples are polycrystalline. All diffraction peaks could be indexed to the single phase of $MgAl_2O_4$ and matched perfectly with the standard pattern of the cubic spinel JCDPS 75-1796. The results suggest that Cd^{2+} doping does not change the crystal structure of $MgAl_2O_4$ and the incorporation of Cd^{2+} in the crystal structure of the host might have been via substitutional reaction possibly on either Mg^{2+} or Al^{3+} sites.[13] There is no detectable trace of impurity such as Al_2O_3, MgO, or CdO-related impurity. As far as the CdO impurities are concerned, our results are apparently consistent with those reported by Chen et al.,[10] which showed that the key to success in synthesizing $(Zn_{1-x}Cd_x)Ga_2O_4$ is to adopt a temperature of ≥950°C so that the volatility of CdO can be effectively minimized. These results indicate that there is a complete formation of spinel phase at the furnace temperature (800°C), and a further calcination treatment is not necessary.

Figure 2 shows the analysis of the Gaussian fits of the highest intense diffraction (440) peak for the host and Cd^{2+}-doped samples. Generally, it is noted that the incorporation of the Cd^{2+} ions into the host lattice influences the diffraction intensity, which suggests that, depending on the Cd^{2+} concentration, the crystalline quality during the growth of the $MgAl_2O_4$ nanocrystals might be improved or reduced.[14] In comparison with the host, there is evidently a slight shifting to the lower diffraction angle when the Cd^{2+} ions are incorporated into the host lattice. Shifting of the diffraction angles to the lower side indicates that the lattice parameters are slightly higher than that of the un-doped $MgAl_2O_4$ sample.[11,15] Vijayalakshmi et al.[11] observed a similar kind of an increase in the *c* lattice parameter value of ZnO:Cd^{2+} films from 5.19 (for pure ZnO) to 5.22 Å (for 25% Cd^{2+}-doped). This increase in the *c* parameter value were attributed to the substitution of the smaller Zn^{2+} ions (ionic radius 0.74 Å) by the larger Cd^{2+} ions (ionic radius 0.97 Å) in the hexagonal wurtzite ZnO structure. As far as our results are concerned, this increase or expansion in lattice parameters can be explained by considering the ionic radius of Cd^{2+} (0.97 Å),[11] Mg^{2+} (0.72 Å)[16] and Al^{3+} (0.53 Å).[14] Clearly, it can be observed that the replacement of Mg^{2+} or Al^{3+} by Cd^{2+} will cause an expansion of the lattice parameters. However, and due to the ionic radius mismatches, we believe that the Cd^{2+} replaces the Mg^{2+} in the crystal structure of $MgAl_2O_4$. The reason being the fact that it will be easier for the Cd^{2+} to settle on the bigger Mg^{2+} sites compared to the smaller Al^{3+} sites. Therefore, doping Cd^{2+} into the crystal structure of $MgAl_2O_4$ induces the lattice distortion. In our previous results[17] we showed the possibilities of the Cr^{3+} ion occupying two different sites (octahedral and tetrahedral) in the crystal lattice of $ZnAl_2O_4$, which also results in different PL emissions. The average value of the lattice constant *a* of the host and Cd^{2+}-doped spinels as calculated from XRD data was 8.05 Å, which is reasonably very close to the previous reported value of 8.08 Å.[3] The estimated crystallites sizes calculated from the (440) diffraction peak by using Scherrer's equation[18] were found to be 10 nm, 10 nm, 10 nm, 11 nm, and 10 nm for the $x = 0$ (host), 0.25%, 0.75%, 1.5%, and 1.75%, respectively. When comparing the calculated crystallite sizes with Fig. 2 results, it is reasonable to conclude that an increase in (440) diffraction intensity for the sample doped at $x = 0.25\%$ Cd^{2+} is likely due to instrumental error. Although there is a fluctuation of the crystallite sizes for the highly doped samples (i.e., $x = 1.5\%$ and 1.75% Cd^{2+}), we propose that doping at higher concentration is accompanied by an increase in crystallite sizes.

In order to confirm composition of the constituent elements, the powder samples were analyzed with an EDS technique. Figure 3a–c show the EDS spectrum of the un-doped and *x*% Cd^{2+}-doped $MgAl_2O_4$ samples. The EDS analysis for the un-doped sample shown in Fig. 3a indicates the presence of Mg, Al, and O. Figure 3b–c illustrate the samples doped with Cd^{2+} at the lower and higher concentrations, which clearly confirms the presence of Mg, Al, O, and Cd in the $MgAl_2O_4$:Cd^{2+} phosphor. In addition to these peaks, the EDS spectrum shows additional peaks from carbon (C), which is due to the conductive carbon (C) films coated on the

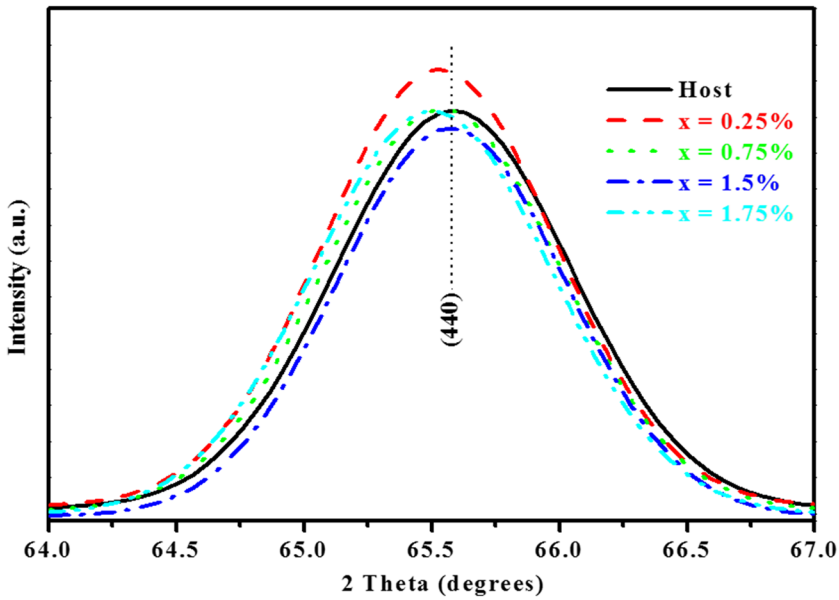

Fig. 2. Analysis of (440) diffraction peak.

samples during the course of EDS measurement. Although EDS cannot be used to determine the dopant concentration in the powder samples, it is interesting to identify that the sample in Fig. 3c is doped with the higher Cd^{2+} concentration compared to the sample in Fig. 3b.

The microstructure of the prepared un-doped and x% Cd^{2+}-doped $MgAl_2O_4$ phosphors were examined using SEM, and the results are illustrated in Fig. 4a–c, respectively. The morphology of all samples remains almost the same. The powder morphology consists of the small crystallites, which are agglomerated together to make bigger crystals. Upon increasing the Cd^{2+} concentration to $x = 1.75\%$, the grains boundary is also observed.

Furthermore, the $x = 0\%$, 0.75%, and 1.75% were examined by HR-TEM as shown in Fig. 5a–f. In all samples, the crystallites are agglomerated, which agrees very well with the SEM results in Fig. 4a–c. Due to the high degree of crystallites' agglomeration, it is not an easy task to predict the accurate crystallites sizes. However, these results show that the average crystallites sizes are below 20 nm, which is reasonable when compared with the values predicted by the XRD results. The lattice fringes for $x = 0\%$, 0.75%, and 1.75% are shown in Fig. 5b, d, and f, respectively. Thus, it is clear that the sol–gel method can produce powder containing nanoparticles. The crystallite sizes from HR-TEM seems to be the same or equal, which is in good agreement with the crystallites sizes calculated from the XRD results. Thus, characteristics of the SEM and HR-TEM results are found to resemble each other on morphology.

UV–Vis diffuse reflection spectroscopy was used to study the absorption characteristics of the un-doped and x% Cd^{2+}-doped $MgAl_2O_4$ powders. Figure 6a compares the UV–Vis spectra of the un-doped and x% Cd^{2+}-doped phosphors. It can clearly be seen that there are three absorption bands located at around 214 nm, 258 nm, and 275 nm. The absorption band at 214 nm (~5.8 eV) is certainly attributed to the band-to-band absorption from the host material. Sampath et al.[19] calculations showed that the band gap of the $MgAl_2O_4$ is 5.8 eV, which is consistent with our current results. In addition, the Paiva et al.[20] results showed that the irradiated $MgAl_2O_4$ crystal presents two optical absorption (OA) bands centred at 3.4 and 5.1 eV. The 3.4 eV band was found to increase with the irradiation-dose and stabilizes its maximum height for doses near 10 kGy. Based on these results[19,20] we infer that it is possible to find the band gap that ranges between 3.4 eV and 5.8 eV for the $MgAl_2O_4$ crystal. The OA band at around 258 nm, which appears at the higher Cd^{2+} concentration, is attributed to the impurities induced by the Cd^{2+} ion. This shift in OA band to the higher wavelength (that is; from 214 nm to 258 nm) suggests that doping at the higher Cd^{2+} concentration decreases the band gap of the host material (see Fig. 6b). We propose that the OA band at 275 nm might possibly be due to the band gap defects within the host material.

The Kubelka–Munk function $K = (1 - R)^2/(2R)$ was used to transform the reflectance to the values proportional to absorbance, and the Tauc plot of $(K \times hv)^n$ against hv[21,22] (with $n = 2$, which is appropriate for a direct band gap material such as $MgAl_2O_4$) is presented in Fig. 6b for the un-doped and Cd^{2+}-doped $MgAl_2O_4$. The optical energy gap (E_g) values of the samples were obtained by extrapolating the graph to the x-axis $(K \times hv)^2 = 0.22$ The results indicate that the band gab of the $MgAl_2O_4$ is

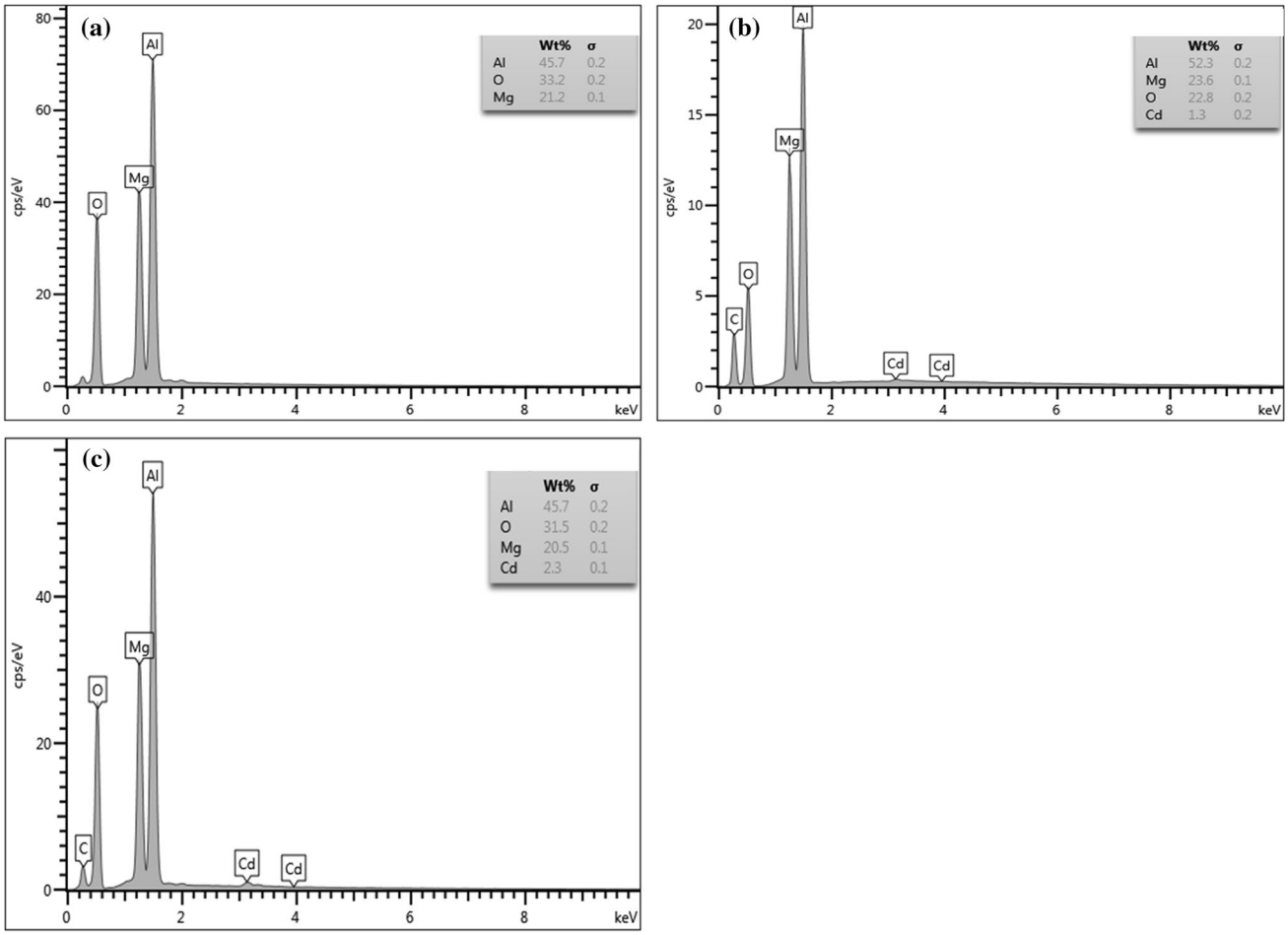

Fig. 3. EDS spectrum of the (a) host, (b) $x = 0.75\%$, and (c) $x = 1.75\%$.

influenced by the Cd^{2+} concentration. At lower Cd^{2+} concentration, the band gap of the host was observed to increase, while at higher Cd^{2+} concentration, it was decreased. The observed higher E_g value at lower Cd^{2+} concentration might be due to the smaller crystallite size (see XRD results). This phenomena could be explained by the fact that the decrease of crystallite size leads to an increasing band gap on the basis of the quantum size effect.[23] In doped semiconductors, there is a possibility of widening of the optical band gap due to the Burstein-Moss (BM) effect, which takes place due to an increase in carrier concentration.[24] The reduction in the band gap at the higher Cd^{2+} doping may be due to the increase in crystallite sizes. A slight fluctuation in E_g value at higher Cd^{2+} concentration observed in Fig. 6b is attributed to the fluctuation of the crystallite size as estimated in the XRD results. Comparable behaviour was observed by Li et al.[23] on the In_2S_3:Tb^{3+} nanophosphor. However, in their study there was a clear increase in crystallites sizes (that is; no fluctuations were observed) with an increase with Tb^{3+} concentration, while the E_g was observed to decrease and vice versa. When comparing the UV–Vis and XRD results, it can be concluded that the E_g value depends on the crystallite sizes, which also depends on the Cd^{2+} concentration. Therefore, these results suggest that the optical band gap of $MgAl_2O_4$ can be engineered or tuned by varying the Cd^{2+} concentration.

The PL excitation and emission spectra of the series $MgAl_2O_4$:$x\%$ Cd^{2+} ($0 < x \leq 1.75\%$) is shown in Fig. 7a. Figure 7b illustrates the deconvolution of the host sample, which suggests that there are three main peaks of excitation when monitoring the emission at 392 nm, and they are located at around 235 nm, 275 nm, and 320 nm with the dominant peak at 275 nm. The excitation peak at 235 nm (~5.2 eV) is attributed to the host material band-to-band excitation (see Fig. 8). The reason being the fact that the UV–vis results presented in Fig. 6b shows that the E_g = 5.1 eV is for the $MgAl_2O_4$. Thus, the UV–vis and PL results agree with each other for the prediction of the band gap of the $MgAl_2O_4$. Remarkably, when the Cd^{2+} concentration is increased, the excitation band at 235 nm seems to be vanishing, which suggests that the band-to-band excitation is not possible at the higher Cd^{2+} concentration. This is in agreement with the shifting of the OA band from lower to the higher

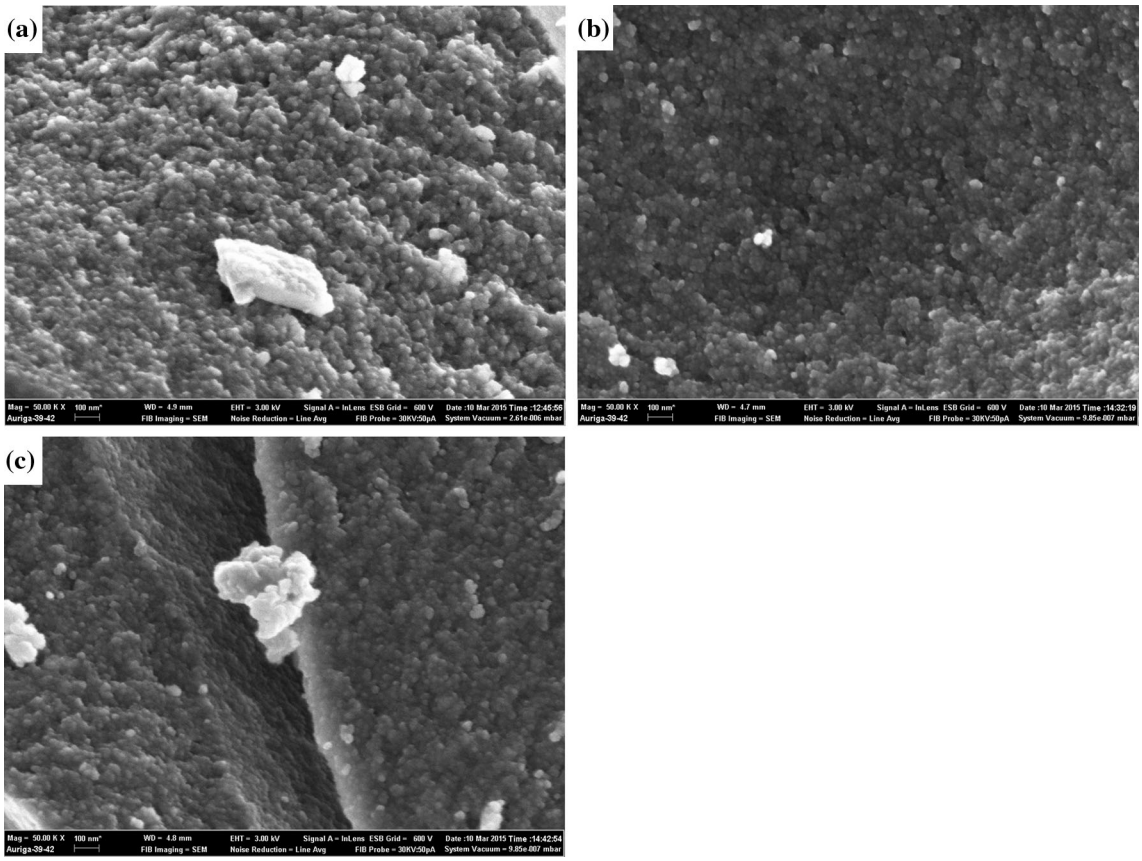

Fig. 4. SEM images of the (a) host, (b) $x = 0.75\%$, and (c) $x = 1.75\%$.

wavelength observed in the UV–vis results in Fig. 6a, which was attributed to the decrease in the band gap of $MgAl_2O_4$ at the higher Cd^{2+} concentration. When considering the XRD results, we believe that the possible reason for that might be due to the greater population of the defects such as oxygen vacancies (V_o^*), which are induced by Cd^{2+} due to the ionic radius mismatches. The excited electrons are trapped via absorption by these defects (V_o^*), and as a result they are forbidden to travel further to the conduction band (CB) and that causes a decrease on the band gap of the $MgAl_2O_4$ host. Thus, the incorporation of Cd^{2+} into the $MgAl_2O_4$ matrix can be interpreted as a development of more new (V_o^*) trapping centres.[25] We have previously reported a similar kind of behaviour in the $ZnAl_2O_4$ spinel doped with Pb^{2+} and Cr^{3+}.[17,26] Excitation peaks at around 275 nm and 320 nm are both attributed to be due to the $MgAl_2O_4$ defects levels (DL) (i) and (ii), respectively, as shown in Fig. 8. The emission spectra of these samples, taken under the same excitation of the 275 nm line are also displayed in Fig. 7a. The results show that there is only one main emission peak located at around 392 nm. Figure 7c presents the normalized emission intensity, which clearly shows that there is no emission peak shifts in all samples, which indicates that the emission is coming from the same channel. That is, an emission peak at 392 nm is attributed to originate from the intrinsic intraband gap defects such as (V_o^*) within the host material, particularly from the defects level (iii) as shown in Fig. 8. In comparison with our previous results,[17,26] the emission from the foreign ions Pb^{2+} and Cr^{3+} as well as the host ($ZnAl_2O_4$) material were concurrently observed. However, it is emphasized that in the current results, there is no emission from the dopant (Cd^{2+} ion). This is motivated by the fact that the conduction electrons can move freely in the particle and some of them may be trapped by the defects within the host material or defect induced by the incorporation of the foreign ion.[27] As far as these results are concerned, it seems reasonable to assume that all of such electrons are easily captured by the defects within the host material (V_o^*) (which are not induced by Cd^{2+}), and that is why there is no observed emission from the Cd^{2+} ion.[27] The luminescence mechanisms taking place can be explained as follows: after the electrons are excited at 275 nm from the valence band (VB) as shown in Fig. 8, they obtain the energy to travel to the higher excited state such as the CB. On their way to the CB, they get trapped into the DL (i) and are de-excited by non-radiative relaxation (NRR) (indicated by the star in Fig. 8) and trapped on the lower DL (ii), which are also de-excited via NRR to the lower DL

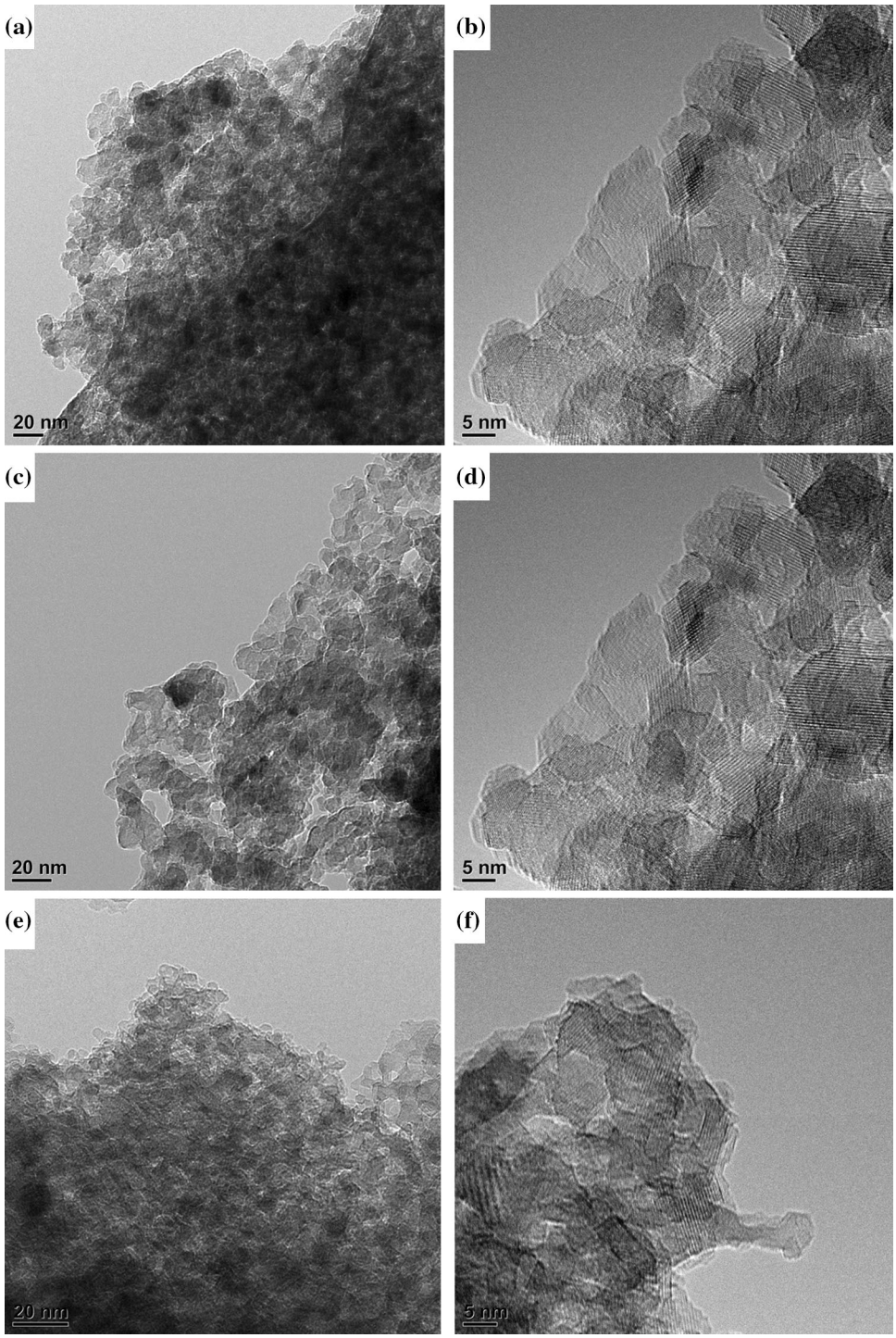

Fig. 5. HR-TEM images of the (a) host, (b) higher magnification of host, (c) $x = 0.75\%$, (d) higher magnification of $x = 0.75\%$, (e) $x = 1.75\%$, and (f) higher magnification of $x = 1.75\%$.

(iii), and then de-excited to the valence band by radiative decay for the observed 392 nm emission. All of these excitations and emission shown in Fig. 7a are summarized in Fig. 8.

From Fig. 7a, it is evident that the emission intensity strongly depends on the Cd^{2+} concentration. The emission intensity as a function of $x\%$ Cd^{2+} is shown in Fig. 7d. The results show that the undoped $MgAl_2O_4$ sample emission intensity is weak, and that is attributed to the insufficient luminescence centres.[17] However, when increasing Cd^{2+} concentration, the emission intensity increases, and the Gaussian fit shows that it reaches the maximal value at $x = 0.88\%$ Cd^{2+}. When Cd^{2+} concentration

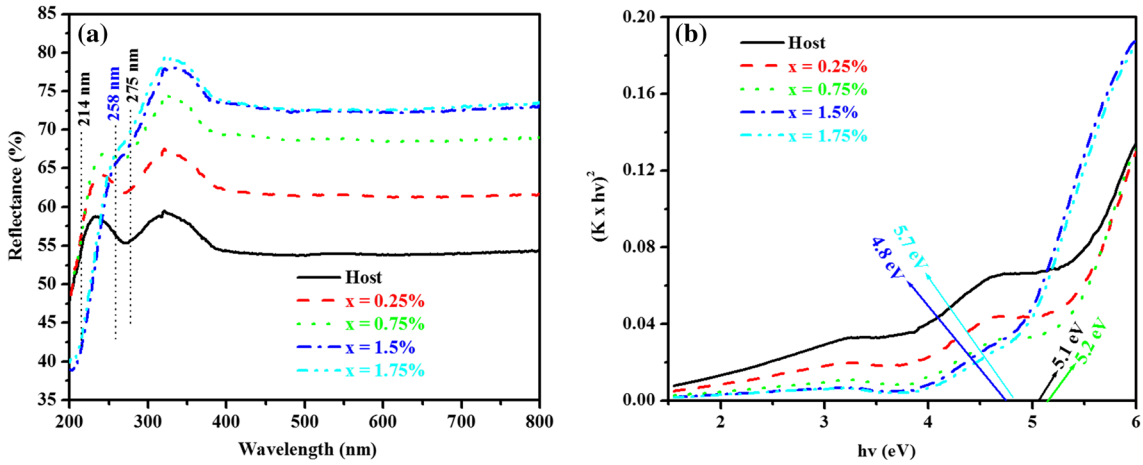

Fig. 6. Diffuse reflectance spectra of the (a) host and x% Cd^{2+}-doped $MgAl_2O_4$ phosphor and (b) plot of $(K \times h\nu)^2$ versus photon energy ($h\nu$) to determine the band gap energy of the prepared nanophosphor samples.

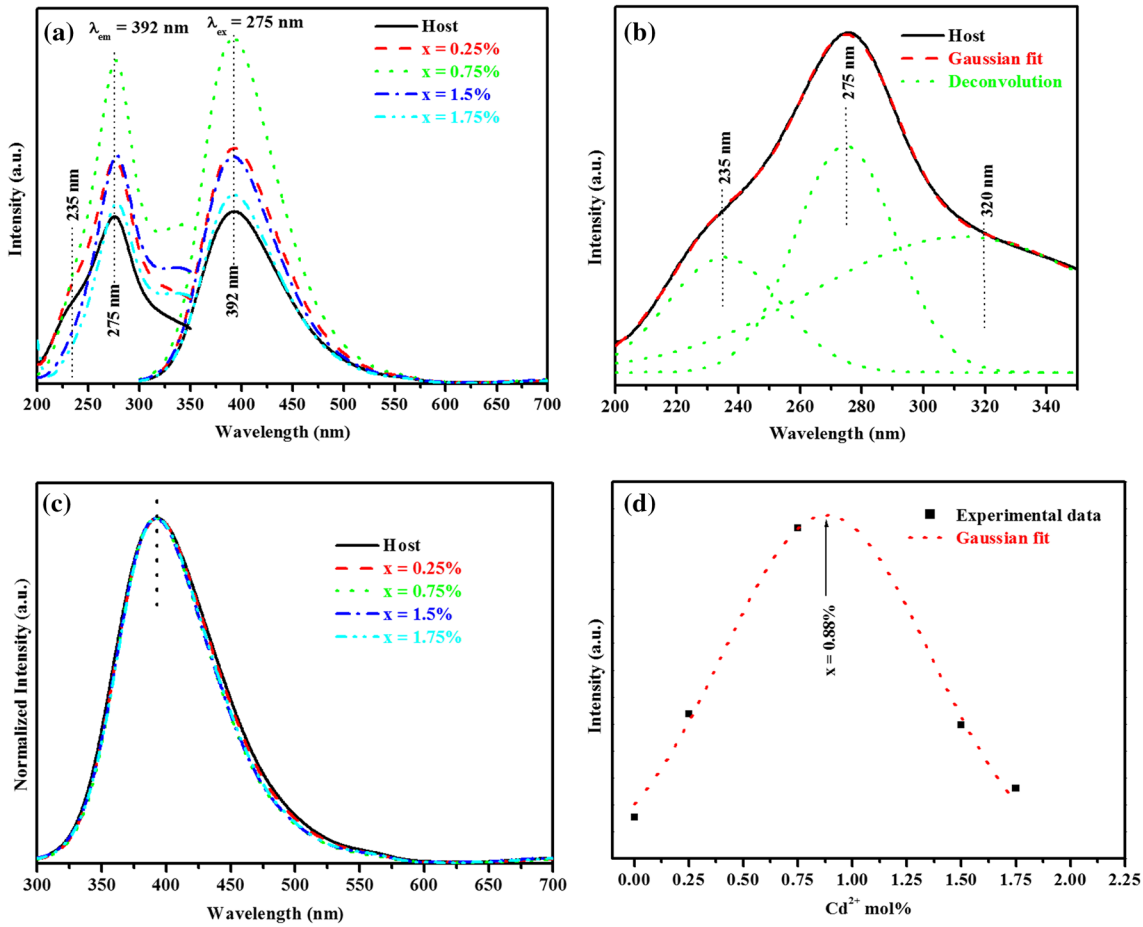

Fig. 7. The excitation and emission spectra of the (a) host and Cd^{2+}-doped $MgAl_2O_4$ phosphor, (b) deconvolution of the host excitation, (c) normalized emission spectra of the $MgAl_2O_4$:x% Cd^{2+}, and (d) emission intensity as a function of x% Cd^{2+} ions.

is increased $x > 0.88\%$ Cd^{2+}, the luminescence intensity starts to decrease, and that is attributed to the well-known concentration quenching.[28] In principle, this phenomena of luminescence enhancement and quenching is normal and anticipated in the doped phosphors.[10,17,26] The concentration quenching is mainly caused by the non-radiative energy transfer, which occurs as a result of an exchange interaction (EI), radiation reabsorption, or multipole–multipole interaction (M-MI).[28,29]

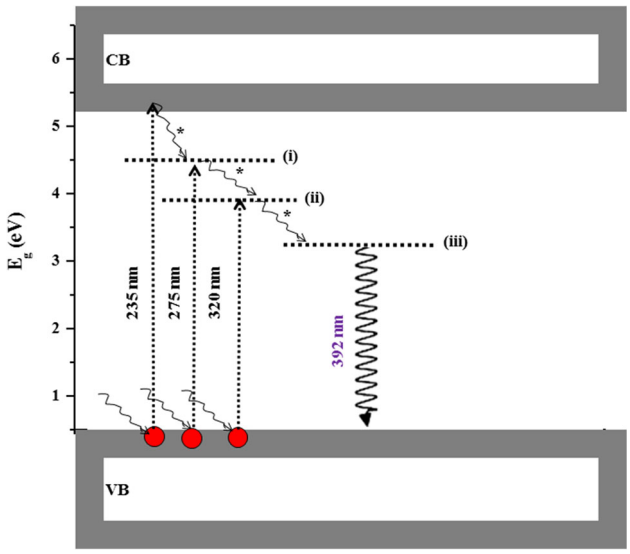

Fig. 8. The proposed excitation and emission pathways mechanism in un-doped and Cd^{2+}-doped $MgAl_2O_4$ phosphor.

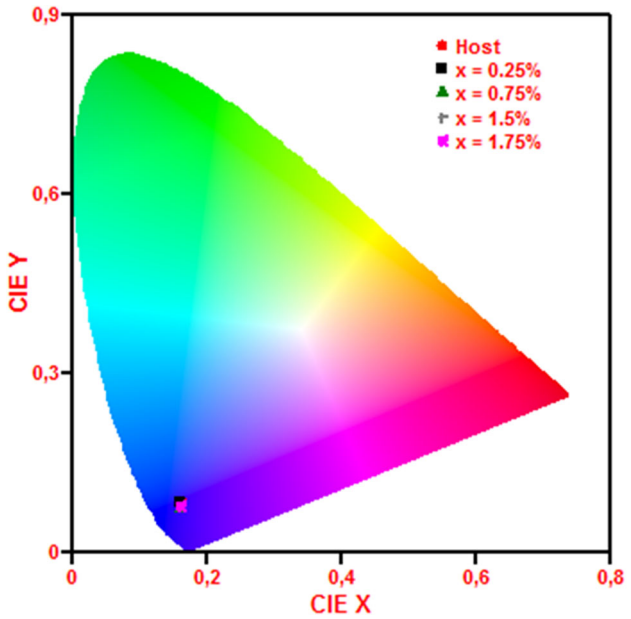

Fig. 9. CIE colour of the series $MgAl_2O_4$:x% Cd^{2+} ($0 < x \leq 1.75$).

According to Blasse,[30] the critical energy transfer distance (R_c) between the neighbouring donors (activators) and acceptors (quenching site) can be expressed by the following relation:

$$R_c = 2\left(\frac{3V}{4\pi X_c N}\right)^{\frac{1}{3}}, \qquad (2)$$

where V is the volume of the unit cell, X_c is the critical concentration of the activator ion, and N is the number of host cations (Mg^{2+}) in the unit cell.[29] In the present host material ($MgAl_2O_4$) and assuming the normal spinel,[4] the value of N is taken as 8, V = 521.7 Å^3 (calculated from the XRD results), and the critical concentration of Cd^{2+} in the $MgAl_2O_4$ (host) is X_c = 0.88. Therefore, the R_c of Cd^{2+} ions is determined to be 5.21 Å. From the broad literature searches, there is no work that has been reported on the R_c of the Cd^{2+}-doped phosphor materials. Hence, this work might probably be the first one. The situation in the RE^{3+} compounds can be characterized as follows[29,31]: If the $R_c < 5$ Å, the exchange interaction becomes the dominant one, and if the value of $R_c > 5$ Å for the rare earth ions indicates that the multipole–multipole interaction (M-MI) is the dominant one, and this is the major cause of concentration quenching of the phosphors material. In this study, it is therefore concluded that the M-MI is the major cause of concentration quenching.[30]

Figure 9 represents the chromaticity co-ordinates of the series $MgAl_2O_4$:x% Cd^{2+} determined using the CIE coordinate calculator software.[32] The software also shows the position of the coordinates in the chromaticity diagram and the expected colour of the material. As shown in Fig. 9, all the samples exhibit violet emission. No change in the emission colour observed might also suggest that the emission is coming from one channel or source. Hence, it is concluded that the emission colour cannot be tuned by varying the Cd^{2+} concentration.

CONCLUSION

The violet emitting $MgAl_2O_4$:x% Cd^{2+} phosphors were successfully prepared by the sol–gel technique. The x-ray diffraction data revealed that all samples consist of a highly crystalline cubic $MgAl_2O_4$ structure. Varying the concentration of Cd^{2+} ions affects the crystallinity of the phosphor. The morphology of the phosphor was not influence by varying the Cd^{2+} concentration. The band gap of the prepared phosphor depends on the crystallite sizes, which are also influenced by the Cd^{2+} concentration. The UV–vis measurements revealed the energy band gap (E_g) value became smaller with the increase of doping concentration. The PL results demonstrated that the violet emission originates from the host material, and there was no evidence of an emission related to the Cd^{2+}. Cd^{2+} doping into the $MgAl_2O_4$ crystal structure was found to increase or populate more defects in the host band gap. Critical energy transfer was found to be 5.21 Å, and the EI was found to be the major cause of concentration quenching. CIE showed that the emission colour could not be tuned by varying the Cd^{2+} concentration.

ACKNOWLEDGEMENTS

This work is supported by the South African National Research Foundation (NRF) Thuthuka Programme (fund number: UID99266).

REFERENCES

1. P. Lombard, B. Boizot, N. Ollier, A. Jouin, and A. Yoshikawa, *J. Cryst. Growth* 311, 899 (2009).
2. G. Slack, *Phys. Rev. A* 134, A1268 (1964).
3. R.C. Peterson, G.A. Lager, and R.L. Hitterman, *Am. Miner.* 76, 1455 (1991).
4. R. Paiva, M. Carvalhaes, and A.R. Blak, *Phys. Stat. Sol. (c)* 4, 1238 (2007).
5. V. Singh, V.K. Rai, S. Watanabe, T.K.G. Rao, L. Badie, I. Ledoux-Rak, and Y.-D. Jho, *Appl. Phys B* 108, 437 (2012).
6. D. Jia and W.M. Yen, *J. Lumin.* 101, 115 (2003).
7. X.Y. Chen, C. Ma, Z.J. Zhang, and X.X. Li, *Microporous Mesoporous Mater.* 123, 202 (2009).
8. A. Jouini, A. Yoshikawa, and Y. Guyot, *Opt. Mater.* 30, 47 (2007).
9. V. Singh, R.P.S. Chakradhar, J.L. Rao, and D.K. Kim, *J. Solid State Chem.* 180, 2067 (2007).
10. T.-M. Chen and Y.-W. Chen, *J. Solid State Chem.* 150, 204 (2000).
11. S. Vijayalakshmi, S. Venkataraj, and R. Jayavel, *J. Phys. D Appl. Phys.* 41, 245403 (2008).
12. S.V. Motloung, F.B. Dejene, H.C. Swart, and O.M. Ntwaeaborwa, *J. Lumin.* 63, 8 (2015).
13. M. Xin, L.Z. Hu, D.-P.Liu, and N.-S. Yu, *Superlattices and Microstructures* 74, 234 (2014).
14. Q. Hou, F. Meng, and J. Sun, *Nano Res. Lett.* 8, 144 (2013).
15. L.F. Koao, F.B. Dejene, R.E. Kroon, and H.C. Swart, *J. Lumin.* 147, 85 (2014).
16. S. Saha, S. Das, U.K. Ghorai, N. Mazumder, B.K. Gupta, and K.K. Chattopadhyay, *Dalton Trans.* 42, 12965 (2013).
17. S.V. Motloung, F.B. Dejene, H.C. Swart, and O.M. Ntwaeaborwa, *Ceram. Int.* 41, 6776 (2015).
18. B.D. Cullity, *1956 Elements of X-ray Diffraction*, 2nd ed. (Addison Wesley, 1978), pp. 285–286.
19. S.K. Sampath, D.G. Kanhere, and R. Pandey, *J. Phys.: Condens. Matter* 11, 3635 (1999).
20. R. Paiva, M. Carvalhaes, and A.R. Blak, *Phys. Stat. Sol. (c)* 4, 1238 (2007).
21. A. Diego, Guzman-Embus, F.M. Vargas-Charry, and C. Vargas-Hernandez, *J. Am. Ceram. Soc*. 1–8, 1 (2015).
22. S.V. Motloung, F.B. Dejene, O.M. Ntwaeaborwa, and H.C. Swart, *Mater. Res. Express* 1, 045029 (2014).
23. Z. Li, P. Wang, T. Yang, H. Yu, B. Xiao, and M. Zhang, *J. Phys. Chem. C* 119, 27688 (2015).
24. M. Anbarasi, V.S. Nagarethinam, and A.R. Balu, *Indian J. Sci.* 13, 48 (2015).
25. P. Borse, W. Vogel, and S. Kulkarni, *J. Colloid Interface Sci.* 293, 437 (2006).
26. S.V. Motloung, F.B. Dejene, H.C. Swart, and O.M. Ntwaeaborwa, *J. Sol-Gel. Sci. Technol.* 70, 422 (2014).
27. J. Beltran-Huarac, J. Wang, H. Tanaka, W.M. Jadwisienczak, B.R. Weiner, and G. Morell, *J. Appl. Phys.* 114, 053106 (2013).
28. H. Tang, H. Berger, P.E. Schmid, F. Levy, and G. Burri, *Solid State Commun.* 87, 847 (1993).
29. G.R. Dillip, B. Ramesh, C.M. Reddy, K. Mallikarjuna, O. Ravi, S.J. Dhoble, S.W. Joo, and B.D.P. Raju, *J. Alloys Compd.* 615, 719 (2014).
30. G. Blasse, *J. Solid State Chem.* 62, 207 (1986).
31. D. Gao, H. Zheng, X. Zhang, W. Gao, Y. Tian, J. Li, and M. Cui, *Nanotechnology*, 22, 175702 (2011).
32. P. Patil (2010). http://www.mathworks.com/matlabcentral/fileexchange/29620-cie-coordinatecalculator.